AIAA JOURNAL
Vol. 36, No. 11, November 1998

Computational Investigation of Shock-Enhanced Mixing: Application to Circular Cross Section Combustor

Sang-Hyeon Lee*
University of Ulsan, Ulsan 680-749, Republic of Korea
and
In-Seuck Jeung† and Youngbin Yoon‡
Seoul National University, Seoul 151-742, Republic of Korea

A computational investigation of shock-enhanced mixing applied to circular cross section combustors is presented. In a circular cross section combustor, there are shock wave intersections at the center axis that produce adverse effects on mixing characteristics. The purpose of this investigation is to analyze the adverse effects due to the shock wave intersections and to develop new combustor geometry minimizing the adverse effects and improving the mixing characteristics. Three-dimensional Navier–Stokes equations are used to calculate the motion of the mean flow. A k–ω turbulence model is used to calculate the turbulent viscosity. It is shown that, in a circular cross section combustor, the shock waves intersecting at the center axis reduce the strength of the longitudinal vorticity and push the fuel downward. A change in the shape of the cross section of the combustor to an octagonal cross section results in a reduction of the adverse effects and an improvement of the mixing characteristics.

Nomenclature

h_i = height of injector nozzle plane
k = turbulence kinetic energy
M = Mach number
p = static pressure
$\bar{p}_0$ = averaged isentropic stagnation pressure
T = temperature
x = distance from injection plane normalized by h_i
Y_{He} = maximum mass fraction of helium
Z_{He} = helium liftoff height normalized by h_i
Γ = circulation normalized by $u_\infty h_i$
μ = viscosity
ρ = density
τ = viscous tensor
ω = turbulent dissipation variable
$\boldsymbol{\omega}$ = vorticity vector

Subscripts

i = injector
s = species
0 = isentropic stagnation
∞ = inlet condition

Superscript

d = binary diffusion

Introduction

THERE are many fundamental problems in developing a hypersonic airplane engine: 1) how to mix fuel and air efficiently, 2) how to maintain a stable flame within the combustor, and 3) how to cool the combustor wall. The combustor is one of the critical components of a hypersonic air-breathing propulsion system. The mixing problem in the combustor is a result of the short residence time of the air within the engine. The residence time of the air in a hypersonic airplane engine is on the order of 1 ms for typical flight conditions. Within this short time, fuel must be injected to penetrate deeply into the airstream and be fully mixed and burned. Another requirement is that the fuel injection needs to have an injection angle that is close to the direction of the airstream because it provides a significant portion of the exit momentum.[1–4]

Various methods have been suggested to satisfy these requirements. For example, the injection of fuel in the direction transverse to the inlet airstream has proved to be a reliable method for low-Mach-number flows. With higher-Mach-number flows, however, too much drag due to the formation of a strong normal shock wave, separated flows, reattachment zones, and wake behind the injection flow makes the method virtually ineffective. Swept injector systems, with a lower angle of injection, have excessive leading-edge heat transfer rates. The method utilizing a shear layer produced by the velocity differences between air and fuel rapidly loses its effectiveness as the Mach number increases and finally reaches a point where mixing is never achieved.[2–6]

To overcome the problems just mentioned, Marble's[4] new concept of shock-enhanced mixing has been introduced. It is well known that longitudinal vorticity is very efficient for mixing of fuel and air in hypersonic flows. The longitudinal vorticity generates large-scale convection flow in the cross-section plane that helps the fuel penetrate deeply into the airstream and be fully mixed with the air. There are many kinds of methods to generate longitudinal vorticity: supersonic swirler injector, delta-wing tab mixer, micropylon injector, periodic excitation, and so on. One of the simplest methods to generate a longitudinal vorticity is shock-enhanced mixing with the aid of baroclinic torques. This mechanism requires a well-designed injector system.[2–4] The mechanism of generating baroclinic torque can be explained by the simplified vorticity equation as follows:

$$\rho \frac{\mathrm{D}}{\mathrm{D}t}\left(\frac{\boldsymbol{\omega}}{\rho}\right) = \frac{1}{\rho^2}\nabla\rho \times \nabla p$$

If the pressure gradient is not parallel to the density gradient in a fluid element, vorticity will be generated. Marble[4] suggested a geometric model exploiting this mechanism to mix fuel and air in hypersonic airplane engines. Figure 1 shows the schematics of shock-enhanced mixing in Marble's model combustor. The model combustor consists of alternating compression ramps and expansion troughs, with the injecting nozzle placed at the end of each ramp. As the flow through the trough is turned parallel to the freestream, an oblique shock wave

Presented as Paper 96-0730 at the AIAA 34th Aerospace Sciences Meeting, Reno, NV, Jan. 15–18, 1996; received Nov. 14, 1997; revision received July 15, 1998; accepted for publication Aug. 1, 1998.

*Instructor, Division of Aerospace Engineering, School of Transportation Systems Engineering. Member AIAA.
†Professor, Department of Aerospace Engineering. Senior Member AIAA.
‡Assistant Professor, Department of Aerospace Engineering. Member AIAA.

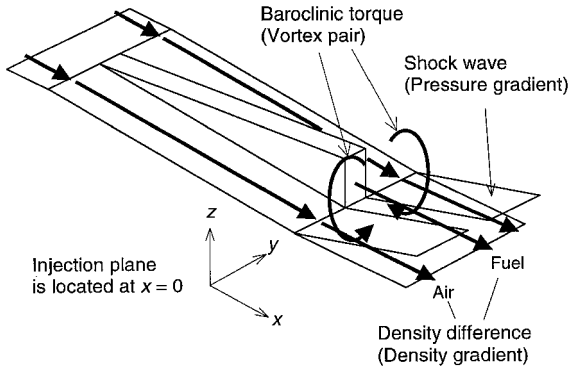

Fig. 1 Schematics of shock-enhanced mixing in planar-type combustor (Marble's[4] model).

is formed, producing the pressure gradient. At the same time, the density gradient perpendicular to the pressure gradient is produced by the density differences between the fuel and air. The torque thus produced is called a baroclinic torque. As a result of the baroclinic torque, two vortices in opposite directions (called a vortex pair) are produced at the two sides of the injector. The vortex pair accelerates the mixing of fuel and air without too much aerodynamic drag and helps the fuel penetrate into the airstream. This method also exploits the injection of fuel to produce thrust. Waitz et al.[7] demonstrated that this model is realistic and efficient for the mixing of fuel and air in a hypervelocity flow. Lee et al.[8] studied the mixing and combustion process of shock-enhanced mixing and showed that the combustion process is dominated by the mixing process and that the proper classification of the mixing regime is the correct way to explain the trends of shock-enhanced mixing.

The primary objective of the present investigation is to analyze the effects of combustor geometry on the mixing characteristics when shock-enhanced mixing is incorporated into a circular cross section combustor. Most scramjet combustors currently being studied have planar-type combustors with a linear array of injector systems because of their convenience in installing on an airplane-type hypersonic vehicle. However, a missile-type hypersonic vehicle would be needed for other types of flight missions. The planar-type combustor loses its effectiveness and convenience for a missile-type vehicle. Hence, alternative combustor geometries need to be considered to satisfy the geometrical constraint of the missile-type vehicle. A potential candidate is a circular cross section combustor with a polar array of injector systems because it could be conveniently installed in a missile-type hypersonic vehicle. In this circular cross section combustor model, the shock waves are generated in a way similar to that in the planar-type model. However, there are shock wave intersections through the center axis in the circular cross section combustor. It was found during the initial stage of this investigation that the intersecting shock waves had adverse effects on the mixing characteristics, resulting in the reduction of the longitudinal vorticity and in pushing the fuel downward. Therefore, analysis of these adverse effects is necessary for a better understanding of shock-enhanced mixing in the circular cross section combustor.

The present work is also intended to propose optimized combustor geometry for a missile-type hypersonic vehicle that minimizes the adverse effects due to the shock wave intersections and improves the mixing characteristics. In the cases of Marble's[4] model and the canonical circular cross section model, the shock wave generated far from the injector does not contribute to the generation of baroclinic torque but only causes stagnation pressure loss. Therefore, optimized combustor geometry is introduced to overcome this problem by eliminating the unnecessary shock waves. The key idea of this combustor is to modify the cross section of the combustor. If the cross-sectional shape of the injection plane is a polygon whose sides are tangential to the inlet circle and the injector systems are placed at each corner, shock wave regions away from the injector can be reduced while the ones near the injector system are kept strong. Consequently, this will lead to an improvement of the mixing characteristics and, in addition, to a considerable reduction of stagnation pressure loss. Any polygon would be a candidate for the cross-sectional shape of the injection plane. However, the diameter of the combustor and shock wave strength needed to generate enough baroclinic torque should be considered to determine the shape of the polygon. In this study, the octagon was chosen as the canonical polygon.

Three types of combustors are investigated for comparison. As a basic model, Marble's planar-type combustor is considered. The second one is the canonical circular cross section model, which has a circular cross section injection plane. The third one is the octagonal cross section model that is a modification of the circular cross section model.

Model Combustors

The combustor geometries and grid systems being studied in this work are shown in Fig. 2, where h_i is injector height, t_i trough length, b_i width of the bottom of the injector, b_w distance between injectors, b_s length of base wedge, α_i angle between injector sides, θ_i angle between injectors, and R radius of the combustor. The dimensions of the three models are presented in Table 1. As the basic model

Table 1 Dimensions of combustors

		Model B		Model C	
Parameter	Model A	B	Bs	C	Cs
h_i, mm	25.40	25.40	25.40	25.40	25.40
t_i, mm	125.40	125.40	125.40	125.40	125.40
b_i, mm	12.70	15.24	15.24	15.24	15.24
b_s, mm	25.40	40.13	24.38	7.62	0.00
b_w, mm	50.80	——	——	——	——
R, mm	——	67.06	45.97	67.06	67.06
α_i, deg	0	10.80	14.58	10.80	10.80
θ_c, deg	——	90	90	90	90

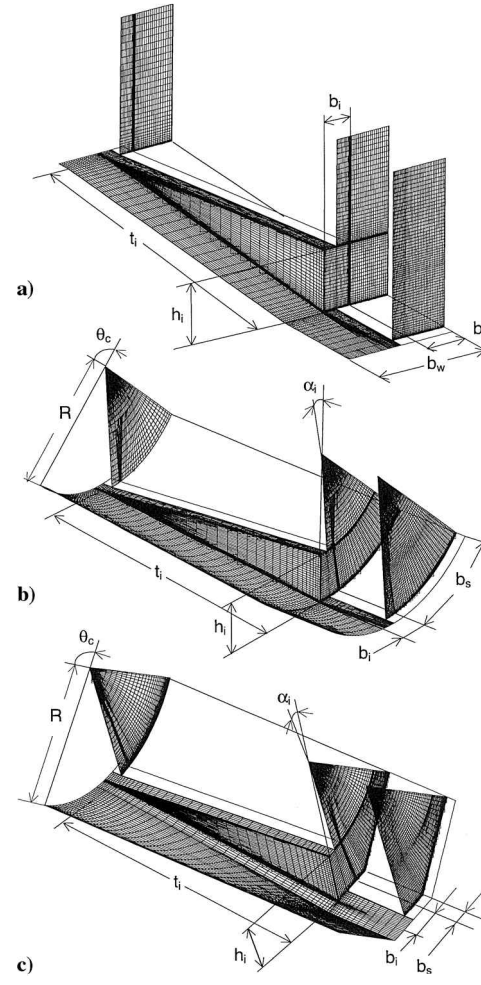

Fig. 2 Geometry and grid systems near injector system: a) model A, b) model B, and c) model C.

utilizing shock-enhanced mixing, Marble's[4] planar-type model was considered. The geometry of this model, which is called model A, is shown in Fig. 2a. The top surface of the injector, which is higher than the inlet surface, generates a shock wave. Hereafter, it is called an injector wedge. The base surface downstream of the injection plane is parallel to the inlet plane; therefore, a shock wave is formed at the position where the base plane begins. Hereafter, it is called the base wedge.

Model B is a canonical model that adopts the mechanism of shock-enhanced mixing to a circular cross section combustor. The cross section of the injection plane is circular. As shown in Fig. 2b, four injectors are placed around the circular wall surface between which the expansion troughs are formed. The shape of the injector is modified to a trapezoidal form with a wider bottom in accordance with the cross-sectional shape of the combustor. Two model B combustors with different diameters were investigated to analyze the size effects.

Model C is an octagonal cross section model suggested to minimize the adverse effects due to the shock wave and its intersection in model B. As shown in Fig. 2c, it is composed of a circular inlet and an octagonal injection plane. The injectors and expansion troughs are placed at the four corners of the cross section. The shapes of the injectors are similar to those of model B. The base wedges exist beside the injector systems but do not exist at the region far from the injector systems. This makes it possible to generate strong shock waves near the injector systems only. Hence, the shock waves not producing baroclinic torque will be reduced in strength, and consequently, the adverse effects due to the shock wave and its intersection would be reduced without reduction of baroclinic torque. To investigate the effects of shock strength, the model without base wedge (model Cs) is studied, and its results are compared with those of the model with base wedge (model C).

The number of grid points of each grid system is 546,000: 210 (axial) × 40 (azimuthal) × 65 (radial). Lee et al.[8] tested this grid system and several others with different numbers of grid points and showed that this number of grid points is sufficient to capture the mixing characteristics of shock-enhanced mixing in Marble's model.

Methods of Calculation

Governing Equations

Three-dimensional Navier–Stokes equations[9–12] were used to solve the mean flow, and the k–ω turbulence model equations[13,14] were used to calculate the turbulent viscosity. These governing equations are expressed in vector form with tensor notation:

$$\frac{\partial Q}{\partial t} + \frac{\partial E_j}{\partial x_j} = \frac{\partial E_{jv}}{\partial x_j} + S_t$$

$$Q = [\rho_s, \rho u_j, \rho e_0, \rho k, \rho\omega]^T$$

$$E_j = [\rho_s u_j, \rho u_j u_k + p\delta_{jk}, (\rho e_0 + p)u_j, \rho k u_j, \rho\omega u_j]^T$$

$$E_{jv} = \left[\rho_s u_{js}^d, \tau_{jk}, \tau_{jk}u_k - q_j, \left(\mu + \sigma^*\mu_t\right)k_{,j}, (\mu + \sigma\mu_t)\omega_{,j}\right]^T$$

$$S_t = \left[0, 0, 0, \left(\tau_{ik}u_{i,k} - \beta^*\rho\omega k\right), (\alpha\omega/k\tau_{ik}u_{i,k} - \beta\rho\omega k)\right]^T$$

In these equations, all viscous and diffusive terms containing derivatives parallel to the body surface are dropped because they are substantially smaller than the viscous terms containing derivatives normal to the wall.[11,12] In the turbulence model equations, the coefficients are taken from those of a standard k–ω turbulence model: $\sigma = \sigma^* = 0.5$, $\alpha = \frac{5}{9}$, $\beta = \frac{3}{40}$, and $\beta^* = \frac{9}{100}$. A model for the dilatation-dissipation term, suggested by Wilcox,[13] is included to predict the compressibility effects, and the coefficients used are the same as those of Wilcox.[13]

The diffusion velocities of the species are found by Fick's law. The formulas and data of viscosity, thermal conductivity, and binary diffusivity are taken from Ref. 15. The intermolecular potential function is the Lennard–Jones 12–6 potential. The viscosity of a pure gas is obtained from the Chapman–Enskog equation, and the viscosity of a gas mixture is calculated using the Wilke method. The thermal conductivity of a pure gas is obtained from the Eucken method, and the thermal conductivity of the gas mixture is calculated with the Wassiljewa equation modified by Mason and Saxena. The diffusivity of a binary gas mixture is obtained from the Chapman–Enskog equation, and the diffusivity of a gas mixture is calculated with Blanc's law. The turbulent diffusivity and turbulent conductivity are obtained from turbulent viscosity. The turbulent Prandtl number and turbulent Schmidt number are both set to 0.9.

A finite volume method is used to discretize the thin-layer Navier–Stokes equations. To obtain the flux vector at the surface of the grid cell, Roe's[16] flux difference splitting scheme is adopted. The lower upper symmetric Gauss–Seidel scheme[17] is used for time integration.

Table 2 Flow conditions of air and helium

Parameter	Air	Helium
M	6.0	1.7
p_0, MPa	6.9	0.023
T_0, K	520	220
p/p_∞	——	1.0
u/u_∞	——	1.0

Flow Conditions

For the purpose of comparing the results of this investigation with previous results, the computational and experimental results of Waitz et al.[7] were considered. In that experiment, helium replaced the hydrogen fuel for the sake of safety; the properties of helium are similar to those of hydrogen fuel. Hence, helium was used as an injectant in this investigation. The flow conditions are shown in Table 2. The Mach numbers of air and helium were 6.0 and 1.7, respectively. The air and helium were treated as perfect gases. The velocity ratio u/u_∞ and the pressure ratio p/p_∞ are both unity. Hence, there should be little shear layer mixing.

Results

Flowfield and Mixing Process

The mixing process with shock-enhanced mixing is governed by the interaction between the shock wave and the flowfield: i.e., the flow acceleration by the baroclinic torques and by the wave itself. To check the differences of mixing characteristics among the three models, the pressure fields and the velocity vector fields are plotted in Fig. 3. The left-hand side of each cross section represents the pressure contours; the maximum value K is 1.7 atm, the minimum value 1 is 0.1 atm, and the increment between symbols is 0.08 atm. The right-hand side represents the velocity vector field in the y–z plane. The first cross-sectional view of each model shows the generation of longitudinal vorticity by the flow expansion from the injector wedge to the expansion trough. In models A and B, a strong downward flow is generated by an expansion wave, whereas a relatively weak downward flow is generated in model C. The second cross-sectional view of each model shows the formation of the shock wave and the longitudinal vorticity. A strong shock wave is formed beside the injector, and it produces the baroclinic torque. Therefore, the fuel–air mixing can be promoted with the aid of the vorticity generated by the injector ramp and the baroclinic torque. In models A and B, a strong shock wave is spread over whole wall, whereas a relatively weak shock wave is formed near the injector system in model C. The third cross-sectional view ($x = 9.0$) of each model shows the downstream flowfield. The flow passing over the injector wedge goes through the expansion wave generated at the end of the injector wedge and is deflected downward. The downward flow impinges against the upward flow of the vortex pair and hinders the penetration of fuel into the airstream. In model B, a strong downward flow is produced over the fuel region, whereas a relatively weak downward flow is produced in model C. Therefore, the center of the vortex pair is hindered more strongly from penetration into the airstream in model B than in model C.

The pressure contours and fuel mass-fraction contours are plotted in Fig. 4 to clarify the general trends of mixing characteristics in the three models. The number under each cross section is the distance from the injection plane normalized by the injector height. The left-hand side of each cross section shows the helium mass-fraction contours; the maximum value is 1.0, and the minimum value is

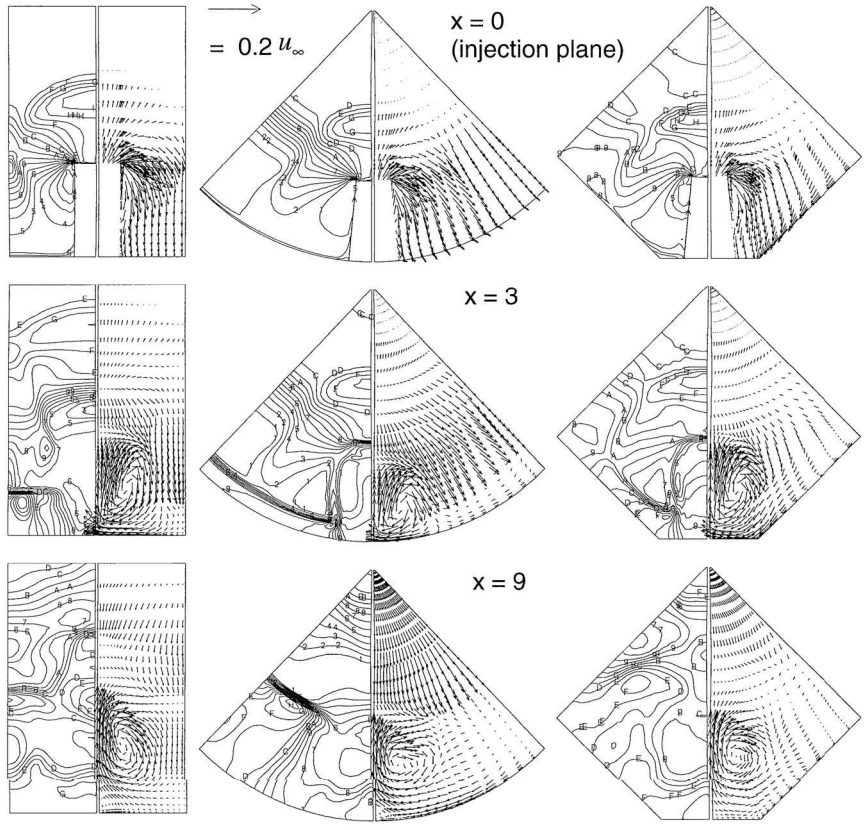

a) Model A **b) Model B** **c) Model C**

Fig. 3 Flowfield near injector system in models A, B, and C.

about 0.05. The right-hand side shows the pressure contours; the maximum value is about 1.7 atm, the minimum value is about 0.4 atm, and the increment between symbols is 0.08 atm. Two shock waves are induced: one by the injector wedge and the other by the base wedge at the end of expansion trough. The fuel shape can be explained by the vortex pair and the relative position between the fuel and the waves. In the near field of the injection plane, the lower part of the fuel shrinks due to the airflow entrained into the fuel region with the aid of the vortex pair, and the upper part of the fuel is blocked by the downward expansion flow over the fuel (Fig. 3). Hence, the fuel shape is elongated in the lateral direction. After the fuel passes away from the waves, the fuel shape is determined by the vortex pair. Hence, the fuel is divided into two regions and penetrates into the airstream with small changes of shape, as described by Lee et al.[8] In the model A case (Fig. 4a), there are no intersections or reflections of shock waves because the upper boundary is treated as the freestream. As the fuel passes away from the shock wave, the fuel penetrates linearly into the airstream due to the vortex pair. In models B and C (Figs. 4b and 4c), however, shock wave intersections occur at the center axis of the combustor. The shock waves, after intersection, affect the fuel penetration adversely by pushing the fuel downward. Although the shock wave intersection is also observed in model C, the strength of shock waves after intersection is much weaker.

Figure 5 shows the process of shock wave intersection and its effects in more detail for models B and C. The left-hand side of each cross section shows fuel concentrations. The right-hand side shows pressure contours; where the maximum value K is 1.7, the minimum value 1 is 0.1 atm, and the increment between symbols is 0.08 atm. The numbers beside the mass fraction contours are the maximum values of the mass fraction of helium. From the pressure contours, shock wave intersections are observed between $x = 15$ and $x = 21$ in models B and C. The strength of the shock wave, after intersection, in model B is stronger than that in model C. The shock wave, after intersection, reaches the fuel around $x = 24$ in models B and C. The flow direction over the fuel region in the y–z plane is changed from upward to downward between the positions before and after the shock wave intersection occurs. The downward flow over the fuel region pushes the fuel downward. The downward flow in model C, however, is weaker than that in model B. Therefore, the decrease in penetration distance in model C is less than that in model B. The last two cross-sectional views show the distortion of the fuel and the reduction of the penetration distance after the shock wave passes through the fuel. This shows that the influence of the shock wave intersection in model C is weaker than that in model B; i.e., the adverse effects are much weaker in model C.

Mixing Characteristics in Circular Cross Section Model (Model B)

The mixing characteristics of the circular cross section model are compared with those of the planar-type model. The present results for model A are compared with the experimental and computational results of Waitz et al.[7] to validate the present computational results. Note that before the comparison the computational results of Waitz et al. were obtained under the assumption of laminar flow. To investigate the effects of combustor size, the mixing characteristics of model B are compared with those of model Bs, which also has a cross-sectional shape but has a diameter about 69% that of model B. The injector height and the injection area of model Bs are the same as those of model B.

Figure 6 shows the histories of the circulations. The circulation is defined as follows:

$$\Gamma = \frac{h_i}{u_\infty} \iint_{y,z} \left(\frac{\partial v}{\partial z} - \frac{\partial w}{\partial y} \right) \mathrm{d}y\, \mathrm{d}z$$

The increase in circulation before the injection plane (negative values of x) is due to the expansion flow from the injector wedge to the trough, whereas the increase in circulation after the injection plane is due to baroclinic torque. There are two peaks at the injection plane near field. The slight decrease after the first peak is believed to be due to the expansion flow over the fuel region (Fig. 3), and the second peak after the first peak is due to the generation of baroclinic torque. The trend of circulation of model A is similar to that of Waitz

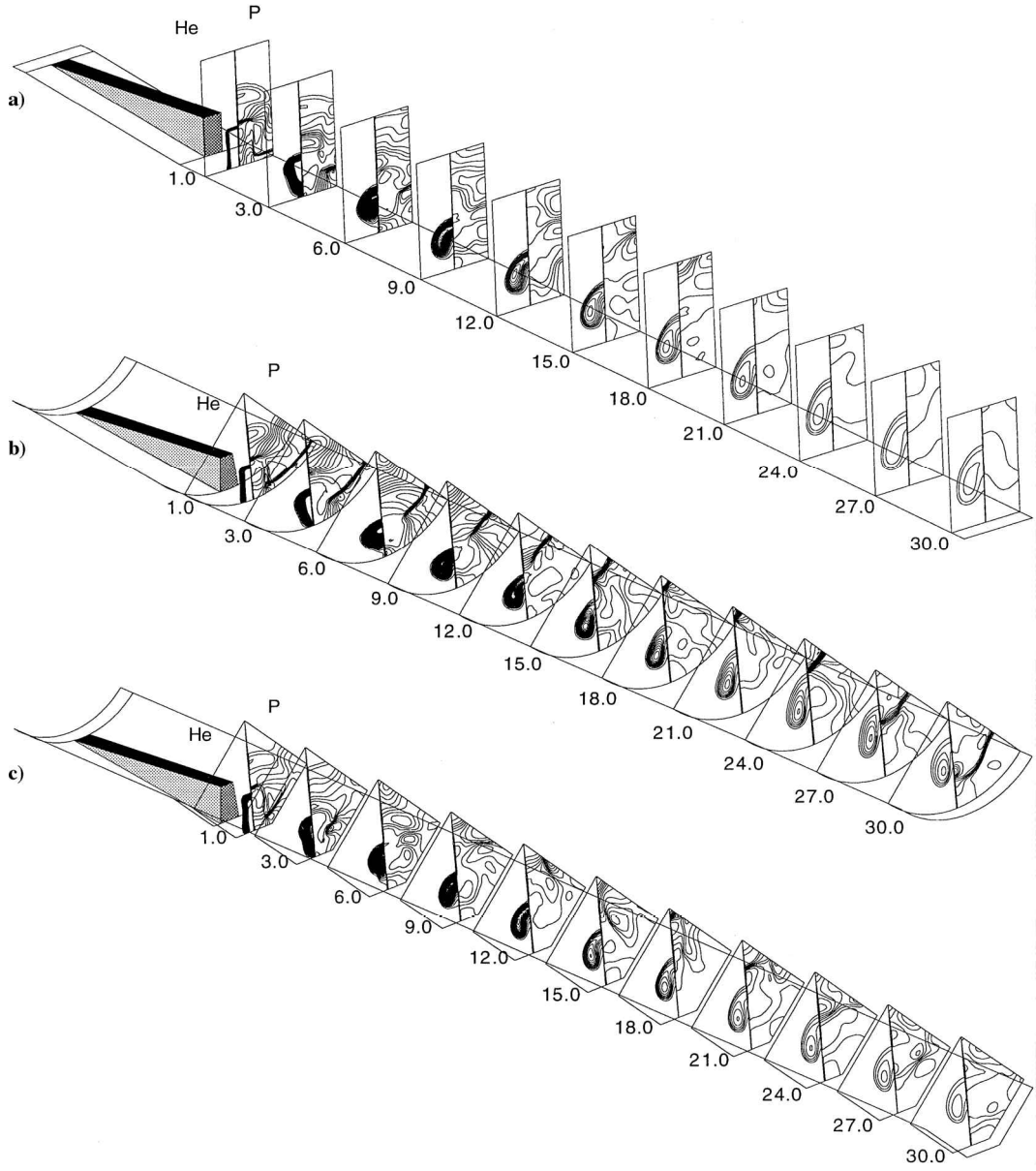

Fig. 4 Global views of flowfield and mixing process: a) model A, b) model B, and c) model C.

et al.,[7] although the present result shows slightly larger values at the injection plane near field and slightly smaller values at the injection plane far field. The slow decay after $x = 7$ is believed to be due to the dissipation under the condition that there is no generation mechanism of baroclinic torque. The circular cross section models (models B and Bs) have trends different from that of the planar-type model (model A); the fluctuations of circulation are found after around $x = 10$ in models B and Bs. It is expected that the increase in circulation in model B after $x = 15$ is due to the high-pressure region under the fuel region, the decrease after the peak around $x = 22$ is due to the shock wave intersection, and the increase after $x = 30$ is due to the shock wave reflected by the combustor wall. The history of circulation in model Bs is similar to those of model B, but the peaks appear earlier than those of model B.

Figure 7 shows the histories of the penetration distances, which are the distances of the mass center of the fuel from the combustor wall. The trend of fuel penetration of model A is similar to the computational result of Waitz et al.[7] Near the injection plane, the fuel penetration is achieved only by the penetration of the lower part of the fuel because the upper part is blocked by the downward expansion flow over the fuel region (Fig. 3), which results in deceleration of the upward flow of the fuel and the reduction of the slope of penetration distance. This flow deceleration of the upward flow produces the high-pressure region under the fuel region. Therefore, the fuel again begins to penetrate into the air after the fuel passes away from the shock waves. Far from the injection plane, the fuel penetrates with a constant slope because there is no flow acceleration mechanism after the fuel passes away from the shock waves. The circular cross section models (models B and Bs) have different trends after $x = 10$ from those of the planar-type model (model A). The increase and decrease in the penetration distance are seen in model B and Bs; these differences are due to the shock wave intersections. Models B and Bs show similar trends in the penetration distances in the early stage, even though they have different penetration distances at the later stage. Model Bs, with a smaller combustor diameter, has an earlier and smaller peak value than model B because the smaller model undergoes earlier shock wave intersection than the larger one. It is, therefore, recommended to use a larger diameter combustor to retard the adverse effects of shock intersection.

Figure 8 shows the comparison of mixing rates on a log-log scale. The mixing rate is estimated by the decay rate of the maximum mass fraction of fuel. The trend of the mixing rate of model A is similar to the experimental result of Waitz et al.[7] This can be explained by the concept of the mixing regime[8]; there are two types of mixing regimes. Near the injection plane, there is a convection-dominated regime due to flow acceleration mechanisms, and far from the injection plane, there is a diffusion-dominated regime due to the disappearance of the significant flow acceleration mechanism. Therefore,

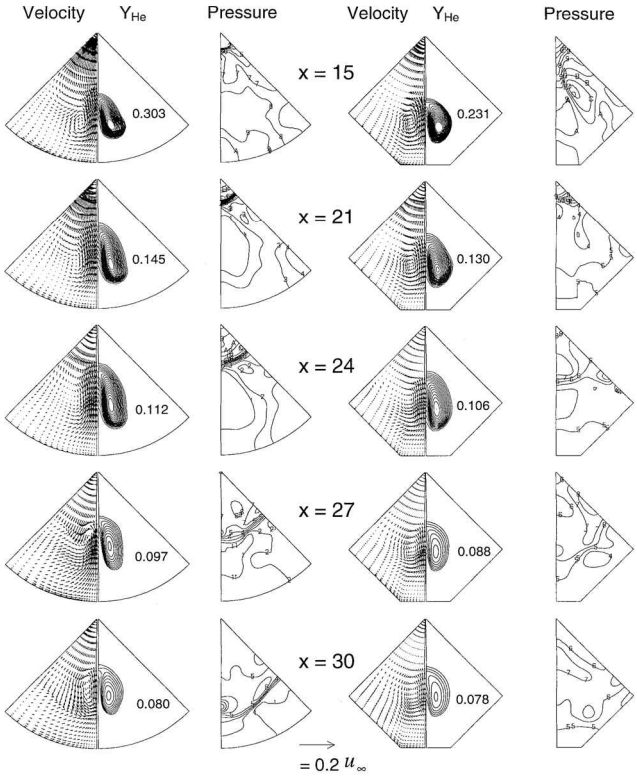

a) Model B **b) Model C**

Fig. 5 Process of shock wave intersection in a) circular-type combustor and b) octagonal-type combustor.

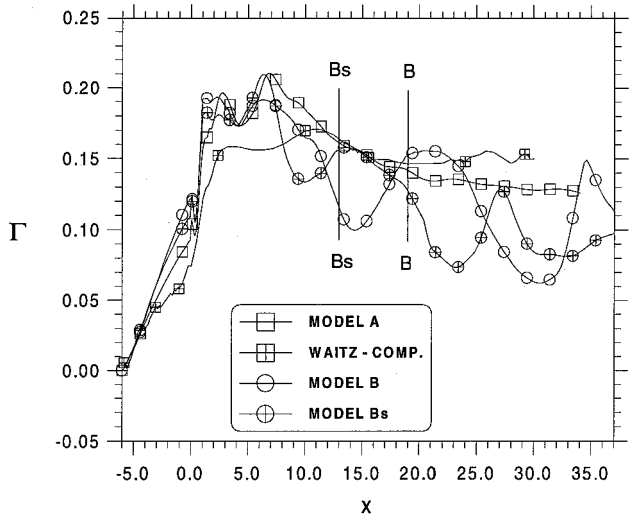

Fig. 6 Comparison of circulation normalized by inlet air velocity and injector height ($u_\infty h_i$); Bs–Bs indicates the position of shock intersection in smaller combustor (model Bs), and B–B indicates the position of shock intersection in larger combustor (model B).

there is an acceleration of the mixing rate near the injection plane, whereas there is linear decay of the maximum mass fraction of fuel far from the injection plane. The present result calculated with the k–ω turbulence model is in good agreement with the experiment result of Waitz et al.,[7] whereas the result calculated with laminar equations does not predict the proper trends. This suggests that an adequate turbulence model should be used to predict the mixing characteristics in shock-enhanced mixing. The circular cross section model (models B and Bs) have trends similar to that of model A, but the mixing rate is inferior because of the smaller circulation value than that of model A. Note that most of the differences in mixing characteristics between the planar-type model and the circular cross section model are caused by the shock wave intersections. The intersected shock waves have adverse effects on mixing characteristics such as the reduction of longitudinal vorticity and the hindrance of the fuel penetration by pushing the fuel downward.

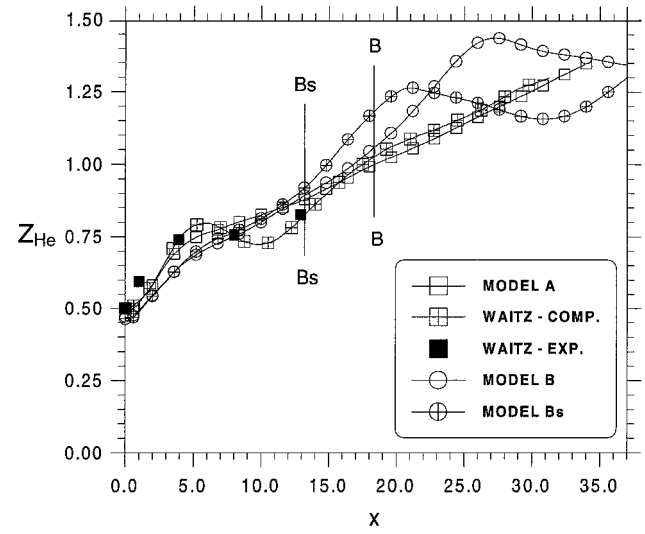

Fig. 7 Comparison of penetration distance normalized by injector height h_i; Bs–Bs indicates the position of shock intersection in smaller combustor (model Bs), and B–B indicates the position of shock intersection in larger combustor (model B).

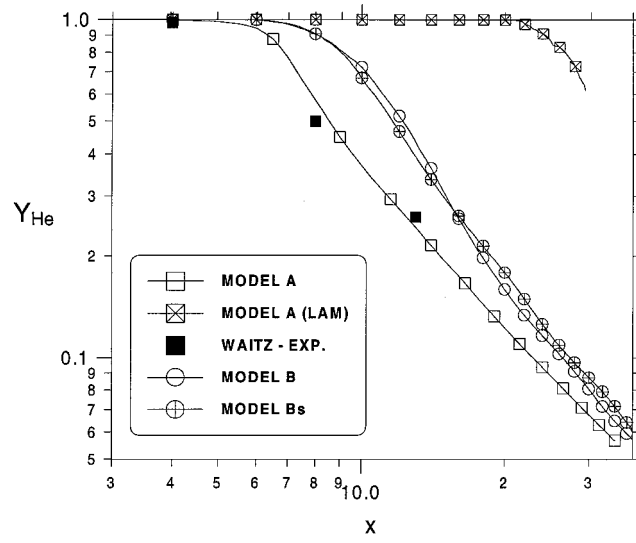

Fig. 8 Comparison of mixing rate expressed by decay rate of maximum helium mass fraction (plotted on log-log scale).

Mixing Characteristics in Modified Model (Model C)

To check the effects on mixing characteristics due to the geometric modification, the mixing characteristics of the modified circular cross section models (models C and Cs) are compared with those of the canonical circular cross section model (model B).

Figure 9 shows the circulations of the modified model (model C). There are no increases in circulation before the injection plane ($x = 0$) in models C and Cs. This is because the flow expansion occurs near the injector system, whereas the flow expansion occurs in a wide range in models A and B (see Fig. 3). The trends of the circulation of models C and Cs are similar to each other, but model C has a larger circulation increase downstream of the injection plane than model Cs because model C has a stronger baroclinic torque, due to the stronger shock wave beside the injection plane, than that of model Cs. Therefore, model C always has higher circulation in all regions after the injection plane than model Cs. There is no sharp decrease in the circulation after the shock wave intersection because the strength of the shock intersection is weaker in models C and Cs than in model B.

Figure 10 shows the penetration distance in the modified model (model C). In the early stage, models C and Cs have higher

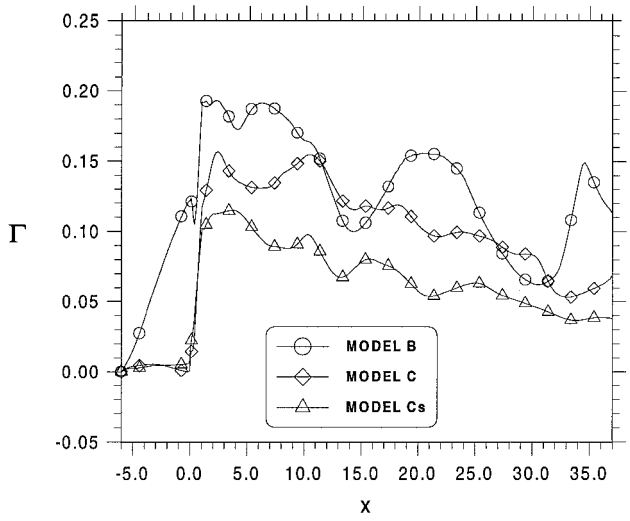

Fig. 9 Comparison of circulation normalized by inlet air velocity and injector height ($u_\infty h_i$).

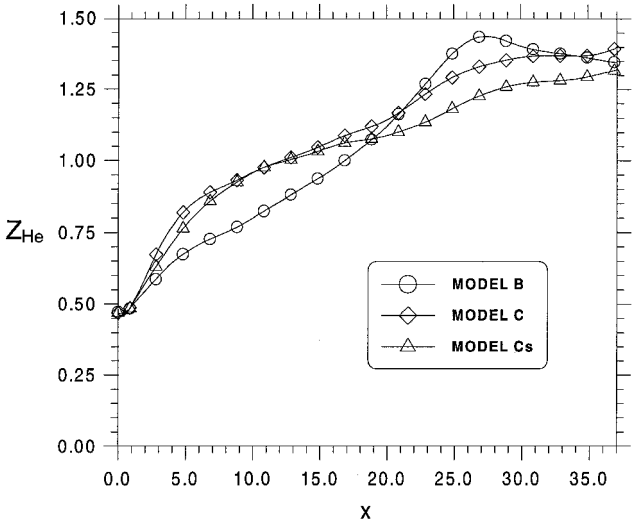

Fig. 10 Comparison of penetration distance normalized by injector height h_i.

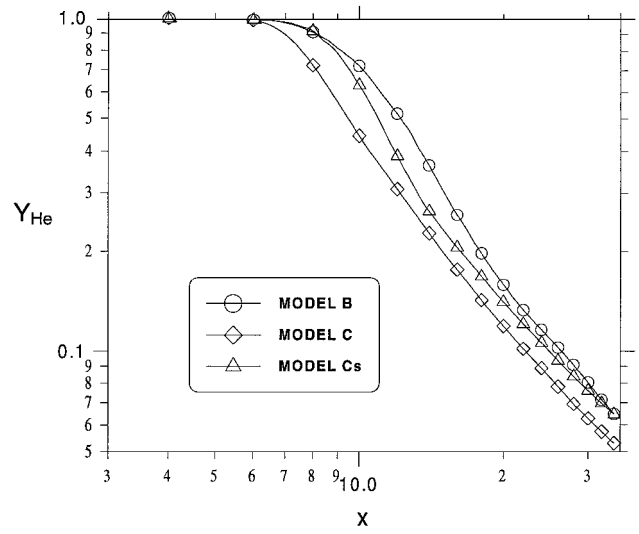

Fig. 11 Comparison of mixing rate expressed by decay rate of maximum hydrogen mass fraction (plotted on log-log scale).

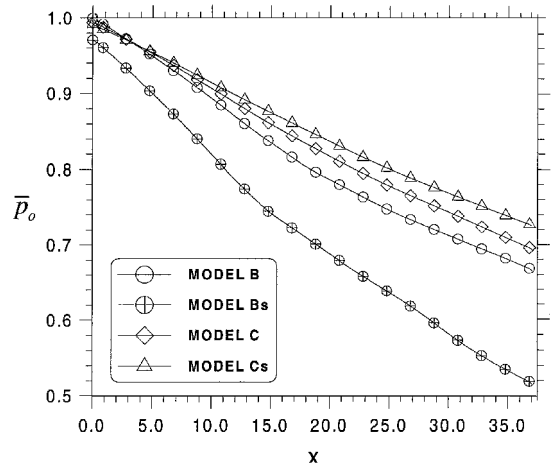

Fig. 12 Comparison of stagnation pressures normalized by stagnation pressure of injection plane of model B.

penetration distances due to the stronger entrainment flow than model B. This is because the downward flow induced by the shock wave due to the injector wedge in model C is weaker than that in model B, as shown in Figs. 3a and 3b. However, the situation is reversed after about $x = 20$. There are no decreases in penetration distances in models C and Cs, whereas there is a decrease in the penetration distance in model B ($x > 25$); i.e., the influences of the shock wave intersection in models C and Cs are weaker than that in model B. Therefore, model C has a higher penetration distance than model B after $x = 32$.

Figure 11 shows the mixing rate in the modified model. The trend in the mixing rate of model C is similar to that of model B; the maximum mass fraction in every model decays linearly on a log-log scale. It seems that the shock intersection does not disturb the trend of the mixing rate. Models C and Cs have higher mixing rates due to the stronger entrainment flow than model B. Comparing models C and Cs, model C has a higher mixing rate. This suggests that the length of the base wedge be longer to obtain a higher mixing rate.

Figure 12 shows the history of the averaged stagnation pressure of models B and C normalized by the averaged stagnation pressure of model B at the injection plane. The averaged stagnation pressure $\bar{p}_0$ is defined in the following form:

$$\bar{p}_0 = \iint_{y,z} p_0 \rho u \, \mathrm{d}y \, \mathrm{d}z \Big/ \iint_{y,z} \rho u \, \mathrm{d}y \, \mathrm{d}z$$

Model C shows less stagnation pressure loss than model B, and model Cs, whose length of the base wedge is zero, shows less stagnation pressure loss than model C. These results suggest that the model with weaker strength of shock waves has less stagnation pressure loss. Model Bs shows much more stagnation pressure loss than model B. This is because the shock strength of model Bs, whose diameter is smaller than that of model B, is relatively stronger than that of model B.

From the analyses of the mixing characteristics between models B and C, it is believed that the geometric modification (model C) gives not only significant improvement of mixing rates but also considerable reduction of stagnation pressure loss. However, in the octagonal cross section models, it is noted that the case with the larger base wedge (model C) shows a better mixing rate but shows higher stagnation pressure loss than the case without the base wedge (model Cs). Therefore, in the octagonal cross section models, the length of the base wedge should be determined appropriately to obtain optimum mixing characteristics.

Conclusions

A computational investigation on shock-enhanced mixing applied to the circular cross section combustor was conducted. The present results of the planar-type combustor model were compared with the computational and experimental results of previous investigations.

In the circular cross section combustor, there are strong shock wave intersections at the center axis. It is shown that the shock waves, after intersection, have adverse effects on the mixing characteristics

such as reducing the longitudinal vorticity and pushing the fuel downward. The diameter of the combustor should be large enough to avoid adverse effects of shock wave intersection and to reduce the stagnation pressure loss.

A geometric modification is introduced to minimize the adverse effects caused by the shock wave and its intersection. The cross section of the injection plane is changed from a circular shape to an octagonal shape to remove unnecessary shock waves away from the injector system. This geometric modification not only results in minimizing the adverse effects due to the shock wave and its intersection but also gives significant improvement of mixing rates and a considerable reduction of stagnation pressure loss. In the comparison between the octagonal models with and without the base wedge (models C and Cs), it is noted that the length of the base wedge should be determined appropriately to obtain optimum mixing characteristics.

Acknowledgments

The authors would like to acknowledge the Korea Science and Engineering Foundation for supporting this research under Contract 961-1005-043-2. The authors highly appreciate the thoroughness of the reviewer's comments.

References

[1]Billig, F. S., "Research on Supersonic Combustion," *Journal of Propulsion and Power*, Vol. 9, No. 4, 1993, pp. 499–514.

[2]Bushnell, D. M., "Hypervelocity Scramjet Mixing Enhancement," *Journal of Propulsion and Power*, Vol. 11, No. 5, 1995, pp. 1088–1090.

[3]Bogdanoff, D. W., "Advanced Injection and Mixing Techniques for Scramjet Combustors," *Journal of Propulsion and Power*, Vol. 10, No. 2, 1994, pp. 183–190.

[4]Marble, F. E., "Hottel Plenary Lecture: Gasdynamic Enhancement of Non-Premixed Combustion," *Twenty-Fifth Symposium (International) on Combustion*, Combustion Inst., Pittsburgh, PA, 1994, pp. 1–12.

[5]Schetz, J. A., and Billig, F. S., "Penetration of Gaseous Jet Injected into a Supersonic Stream," *Journal of Spacecraft*, Vol. 3, No. 11, 1966, pp. 1658–1665.

[6]Papamoschou, D., and Roshko, A., "The Turbulent Compressible Shear Layer: An Experimental Study," *Journal of Fluid Mechanics*, Vol. 197, Dec. 1988, pp. 453–477.

[7]Waitz, I. A., Marble, F. E., and Zukoski, E. E., "Investigation of a Contoured Wall Injector for Hypervelocity Mixing Augmentation," *AIAA Journal*, Vol. 31, No. 6, 1993, pp. 1014–1021.

[8]Lee, S.-H., Jeung, I.-S., and Yoon, Y., "Computational Investigation of Shock-Enhanced Mixing and Combustion," *AIAA Journal*, Vol. 35, No. 12, 1997, pp. 1813–1820.

[9]Hirsch, C., *Numerical Computation of Internal and External Flows*, Wiley, New York, 1990, pp. 408–594.

[10]Anderson, W. K., Thomas, J. L., and Van Leer, B., "Comparison of Finite Volume Flux Vector Splitting for the Euler Equation," *AIAA Journal*, Vol. 24, No. 9, 1986, pp. 1453–1460.

[11]Wadawdigi, G., Tannehill, J. C., Buelow, P. E., and Lawrence, S. L., "Three-Dimensional Upwind Parabolized Navier–Stokes Code for Supersonic Combustion Flowfield," *Journal of Thermophysics and Heat Transfer*, Vol. 7, No. 4, 1993, pp. 661–667.

[12]Hoffmann, K. A., *Computational Fluid Dynamics for Engineers*, Engineering Education System, Austin, TX, 1989, pp. 306–369.

[13]Wilcox, D. C., *Turbulence Modeling for CFD*, DCW Industries, La Cañada, CA, 1993, pp. 73–212.

[14]Patel, V. C., Rodi, W., and Scheuerer, G., "Turbulence Models for Near-Wall and Low Reynolds Number Flow: A Review," *AIAA Journal*, Vol. 23, No. 9, 1986, pp. 1308–1319.

[15]Reid, C. R., Prausnitz, J. M., and Poling, B. E., *The Properties of Gases and Liquids*, 4th ed., McGraw–Hill, New York, 1988, pp. 388–631.

[16]Roe, P. L., "Approximate Riemann Solvers, Parameter Vectors, and Difference Schemes," *Journal of Computational Physics*, Vol. 43, No. 3, 1981, pp. 352–372.

[17]Yoon, S., and Jameson, A., "Lower-Upper Symmetric-Gauss–Seidel Method for the Euler and Navier–Stokes Equation," *AIAA Journal*, Vol. 26, No. 9, 1988, pp. 1025, 1026.

K. Kailasanath
Associate Editor